

Bonding Pathways of Gold Nanocrystals in Solution

Zainul Aabdin,^{†,‡,§,||} Jingyu Lu,^{†,‡,§,||} Xi Zhu,[⊥] Utkarsh Anand,^{†,‡,§} N. Duane Loh,^{†,§} Haibin Su,^{*,†} and Utkur Mirsaidov^{*,†,‡,§,||}

[†]Department of Physics, National University of Singapore, 2 Science Drive 3, Singapore, 117551

[‡]Graphene Research Centre, National University of Singapore, 6 Science Drive 2, Singapore, 117546

[§]Centre for Bioimaging Sciences and Department of Biological Sciences, National University of Singapore, 14 Science Drive 4, Singapore, 117543

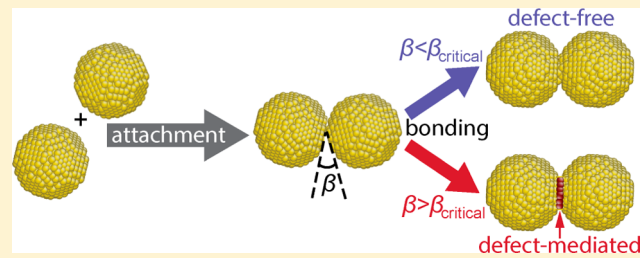
^{||}NUSNNI-Nanocore, National University of Singapore, 5A Engineering Drive 1, Singapore, 117411

[⊥]Division of Materials Science, Nanyang Technological University, 50 Nanyang Avenue, Singapore, 639798

S Supporting Information

ABSTRACT: Nanocrystal bonding is an important phenomenon in crystal growth and nanoscale welding. Here, we show that for gold nanocrystals bonding in solution can follow two distinct pathways: (1) coherent, defect-free bonding occurs when two nanocrystals attach with their lattices aligned to within a critical angle; and (2) beyond this critical angle, defects form at the interfaces where the nanocrystals merge. The critical misalignment angle for ~10 nm crystals is ~15° in both *in situ* experiments and full-atom molecular dynamics simulations. Understanding the origin of this critical angle during bonding may help us predict and manage strain profiles in nanoscale assemblies and inspire techniques toward reproducible and extensible architectures using only basic crystalline blocks.

KEYWORDS: Crystal bonding, *in situ* TEM, nanoparticles, nanocrystals, crystal defects



Crystal bonding, welding of the interface between two or more crystals, plays an important role in structural organization for bottom-up fabrication and synthesis of new materials.^{1–7} Popular building blocks of such materials, nanocrystals,⁸ are often synthesized using combinations of solution reagents⁹ where both solvent and solute have sufficient translational and rotational freedom to explore configurations that result in crystal nucleation and growth. This same spatial freedom in solution also produces rich interparticle dynamics such as nanocrystal coalescence^{6,10} and bonding,^{11,12} which without external forces are thought to prefer pathways that minimize crystal surface energies.^{13,14}

When two crystals bond, the lattice planes across their bonding interfaces can be coherently ordered and defect-free, owing to oriented attachment,¹⁵ or contain defects due to lattice misalignment.¹⁶ In certain situations, the defects created from crystal–crystal bonding can be transient: line dislocations from misoriented attachment can anneal in seconds^{11,17} or be eliminated due to atomic diffusion within the nanocrystal.¹² However, the defects that inevitably develop in most crystalline materials have lasting macroscopic consequences that can affect their growth kinetics,¹⁸ provide critical sites for nucleation,¹⁹ and/or are responsible for changes in material rigidity.^{20,21}

The mesoscopic mechanisms behind defect formation and persistence during crystal synthesis and bonding in solution are still poorly understood. For instance, it is unclear how well crystals need to be aligned for coherently ordered defect-free

bonding. Further, the likelihood of coherent bonding over defect-mediated bonding for nanocrystals in solution, key for manipulating mesoscopic structure, and the role of defects here remain unresolved. Here, we resolved the mechanisms underpinning these phenomena using liquid-cells developed for time-resolved electron microscopy and validated our understanding using simulations in molecular dynamics.

Nanocrystal bonding was observed in solutions contained within liquid cells, which protected the specimen from the high-vacuum within the transmission electron microscope (TEM). This cell comprised of two 20 nm-thick electron translucent SiN_x membranes that sandwiched a thin layer of the specimen (~100 nm).^{6,22–25} Approximately 400 nL of aqueous precursor solution containing 1 mM of HAuCl₄ and 1 mM of cetyltrimonium bromide (CTAB) surfactant was loaded into this liquid cell, which was in turn mounted onto a specimen holder that was inserted into the TEM.²⁶ The nanocrystals are formed in solution spontaneously prior to or during imaging due to reduction of gold ions by electron beam.⁶ The dynamics of nanocrystal bonding is imaged with a JEOL 2010 FEG TEM operating at an electron accelerating voltage of 200 kV with the electron dose rate of 5000–20 000 e/(Å² × s) that initiates

Received: August 27, 2014

Revised: October 1, 2014

Published: October 9, 2014



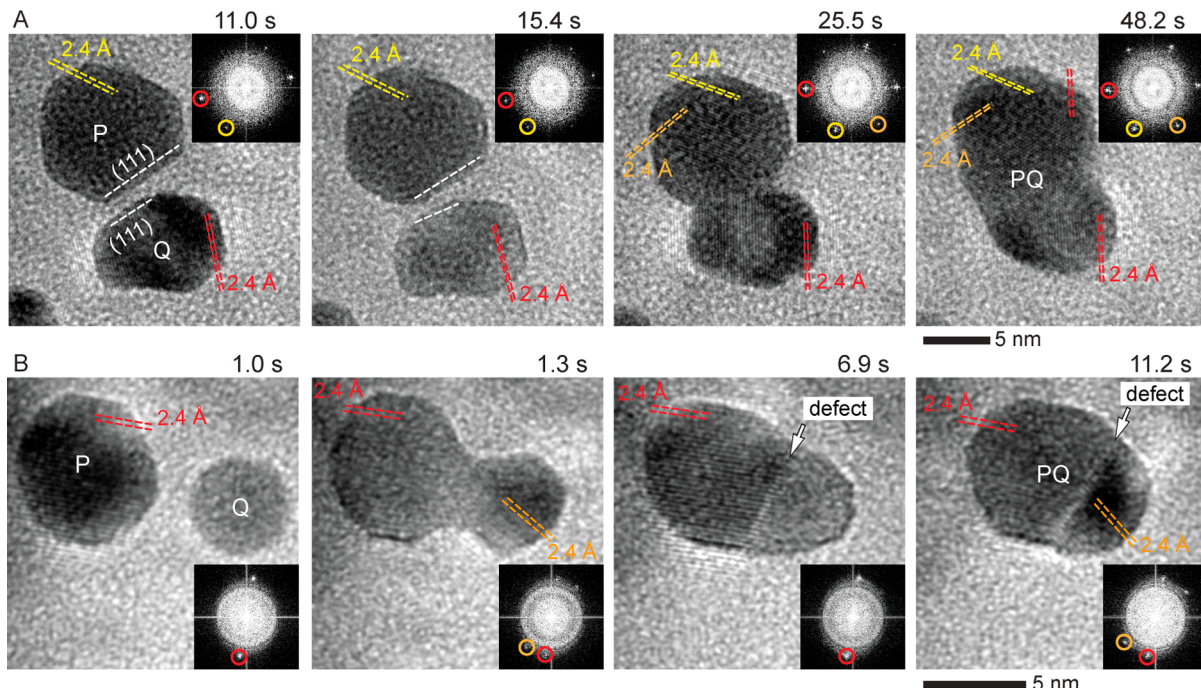


Figure 1. Time-resolved images of coherent and defect-mediated bonding between two gold nanocrystals in solution. (A) Coherent bonding between two gold nanocrystals (*P* and *Q*) sharing a common (111) lattice plane that contact along [111] direction with only $\sim 9^\circ$ misalignment. (B) Two gold nanocrystals with common (111) lattice planes misaligned by 32° at contact yields a nanocrystal *PQ* with defect at the bonding interface. Lattices fringes along (111) plane with 2.4 \AA spacing are marked by dashed parallel lines with corresponding reflections circled in the Fourier transform of the image as shown in the inset (Supporting Information Videos S1–S2).

movement of gold nanocrystals.²⁷ The movement of the nanocrystals is substantially damped due to their interaction with membrane surface.^{28–30} We recorded movies of more than a hundred gold nanocrystal bonding events in solution with many of them at $\sim 2 \text{ \AA}$ lattice resolution on a CCD camera of 10 Hz frame rate.³⁰ Because the presence of large amount of gold in precursor solution may affect the bonding, we restricted our analysis to the nanoparticles with the stable size where the gold in precursor solution has been mostly depleted. This assumption is consistent with the recent study by Schneider et al., where they have shown that for electron flux of $> 2 \times 10^3 \text{ e}/(\text{A}^2 \times \text{s})$ precipitation of gold if present in precursor solution would lead to growth of nanocrystals.³¹

We first examine the case where defects are not expected to form, that is, coherently ordered bonding of two nanocrystals. Figure 1A shows the coherent bonding of two nanocrystals initially separated by $\sim 1 \text{ nm}$, and their (111) lattice planes misaligned by 7° (at $t = 11.0 \text{ s}$). As the nanocrystals approach each other, their lattice misalignment first increases to 15° (Figure 1A, $t = 15.4 \text{ s}$), decreases to 9° upon contact, then visibly realigns into coherent bonding (Figure 1A, $t = 25.5$ and 48.2 s) (Supporting Information Video S1). The possible reason for oscillation in orientation angle during the approach is the solvation forces that result from hydrodynamic liquid squeezing between two nanocrystals as they approach.³² We tracked the nanocrystal orientations throughout this process by identifying the Fourier reflections belonging to their lattice planes before and after bonding. Here, the bonding was coherent because the reflections of the nanocrystals merged into a single set of monocrystalline reflections with no visible defects (Figure 1A, inset of panel for $t = 48.2 \text{ s}$). Notice that realignment occurs only after crystal–crystal contact, where solvent-mediated forces become less important.

Expectedly, defect-mediated bonding occurs when two nanocrystals meet with their (111) lattice planes initially misaligned by a large angle, for example, by about 32° in Figure 1B (Supporting Information Video S2). Here the nanocrystals do not realign upon bonding and a visible defect plane forms at their merging interface (Figure 1B, $t = 6.9 \text{ s}$, black arrow). Post bonding images and the corresponding splitting in Fourier reflections show that the newly formed nanoparticle is not a single crystal (Figure 1B, $t = 11.2 \text{ s}$). These defects formed during bonding persist for many seconds (Supporting Information Figure S2–S3) and can move within the nanocrystal (Supporting Information Figure S2).

The coherent and defect-mediated bonding sequences captured in Figure 1 are remarkable because upon contact the nanocrystals can reorient themselves to a limited extent, either to achieve coherent bonding when the two nanocrystals are initially slightly misaligned, or rotate to a mutual configuration that allows defects to form. Nanocrystals in the latter case do not further rotate into the former coherently ordered bonding state although, as we shall later show, the former has a substantially lower energy. To validate this hypothesis, we identify the dominant energy considerations here *in silico* with molecular dynamics (MD) simulations (see Supporting Information). Full atomistic simulations at short time scale has proven capable of investigating structural evolution of nanocrystals in the experimental observations typically at seconds to minutes time scale.^{33,34}

To analyze the experimentally observed features in our gold nanocrystals, we model them as crystalline polyhedra that are 10 nm in diameter in our MD simulations. The centrosymmetry metric developed by Kelchner et al.³⁵ is employed to identify the face-centered cubic, body-centered cubic, hexagonal close-packed (hcp) structural units, and an assortment of

crystal defects. This metric quantifies the local broken centrosymmetry at an atomic site, which is characteristic of most lattice defects. As an example, there exists a face-centered cubic stacking fault that corresponds to an hcp-like arrangement of neighbors with broken centrosymmetry.

In our simulations, when close-packed (111) planes of the two gold nanocrystals are perfectly aligned, a coherent, defect-free junction rapidly forms between them (Figure 2A,B) when

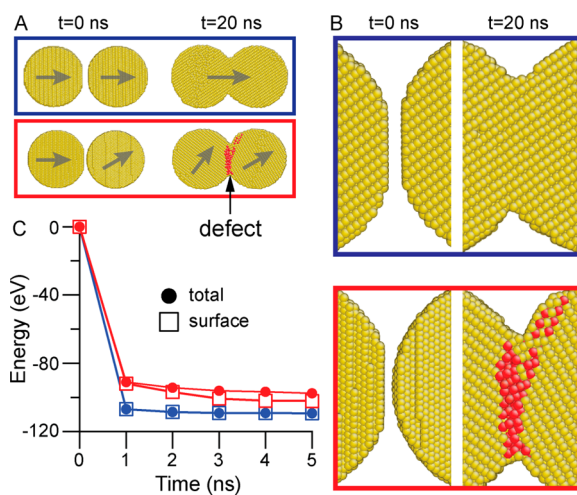


Figure 2. Molecular dynamics simulations of the bonding between two 10 nm gold nanocrystals. (A) Cross-sectional view of structural evaluation of perfectly oriented coherent (blue box) and misaligned (30°) defect-mediated bonding (red box). Gray arrows indicate the orientation of close-packed (111) planes, and defect atoms are colored red. (B) Magnified view of the bonding interface for coherent (blue box) and defect-mediated (red box) bonding. Defects (as defined in the text) are indicated by red atoms. The nanocrystals rotate during defect-mediated bonding. (C) Change in total (solid circles) and surface energies (open squares) for the system of two nanocrystals undergoing coherent (blue) and defect-mediated (red) bonding as described in (A) and (B). The difference between the total and surface energies post bonding is primarily due to the defects.

they bond. The same figure shows that the bonding is not merely rigid-body collision, because of a growing neck that forms between the two nanocrystals and due to diffusion of the surface atoms that fill the neck (also observed in experiment Supporting Information Figure S1). For perfectly aligned coherent bonding, the total energy of the system decreases by ~ 100 eV (Figure 2C) due to reduction in its surface energy (Figure 2C).

Extending our MD simulations to two 10 nm polyhedron gold nanocrystals misaligned by a substantial angle of 30° (Figure 2A, red box), defects emerge near the vicinity of the junction during the first 1 ns of their bonding as shown in Figure 2A,B. These misaligned nanocrystals also rotate when they merge (Figure 2A,B) to minimize the overall surface and defect energies. Although it costs energy for each crystal to create defects, the much larger reduction in surface energy from misaligned bonding still results in an overall decrease in the system's energy, evident in Figure 2C (red curve). Thus, even at considerable lattice misalignment, the surface atoms of two nanocrystals can still bond to substantially reduce their surface energies at the expense of creating defects.

Similar to two-crystal bonding, the pairwise bonding of three-crystals is shown in Figure 3. Here, coherent bonding of two nanocrystals followed by defect-mediated bonding against a

third nanocrystal (Figure 3A). First, nanocrystal P and Q bond through a common (111) lattice plane, yielding a defect-free single nanocrystal PQ (Figure 3A, $t = 5.9$ s, $t = 69.1$ s). This newly formed nanocrystal PQ bonds with the third nanocrystal R through the (200) and (111) lattice planes, yielding defects at the contact ($t = 75.2$ s) (Supporting Information Video S3). The defects continue to grow along the merging interface as the nanocrystal R attaches to the right part of nanocrystal PQ through the lattice planes (200) with (111) (Figure 3A, $t = 135.9$ s). MD simulations show that surface energy reduction as the primary driver for bonding three gold nanocrystals together (Figure 3B,C), even when only two gold crystals bond coherently as the third particle forms defects at the bonding interface with those two.

Because in our *in situ* experiments coherent bonding can occur for crystals in solution where their common lattice planes are slightly misaligned during their initial contact (Figure 1A, Supporting Information Figure S4) we extended our simulations to different initial misalignment angles at contact to find the threshold angle of misalignment above which the defects are present during bonding (Figure 4A). We found that the critical angle for misaligned contact for two gold nanocrystals from MD simulations to be between 12° and 14° . Defects appear in the bonding interface only when misalignment angles 14° or larger (Figure 4A, Supporting Information Figure S5). The simulation results are comparable to our *in situ* TEM observations of 64 lattice resolution bonding events, where we consistently see that all bonding events for initial contact angles between (111) common lattice planes of 15° or less lead to defect-free coherent bonding. For angles greater than 15° , we only see defect-mediated bonding events (Figure 4B). Because lattice planes remain visible throughout the bonding process, the out-of-plane rotation of nanocrystals with 10 nm in diameter is less than 1° during bonding and this rotation can be neglected (Supporting Information).³⁰ The origin of critical angle shown in Figure 4A is a mismatch between dominant crystallographic lattice orientations and postattachment realignment of nanocrystals driven by reduction in surface energy. When the angle between (111) planes of two gold nanocrystals is less than 15° nanocrystals bond along their (111) common lattice plane. For the angles greater than 15° , the bonding interface between two nanocrystals consists of a mix between (111) and (110) planes (Supporting Information Figure S6), which results in defect formation at bonding interfaces. Our experimental results also reveal that misalignment angles during nanocrystal contact in solution is likely to be small, which subsequently leads to coherent bonding. Coherent bonding occurred for 85% of the cases observed in our experiments (Figure 4B).

The experimental and simulated results in Figure 4 show that there is a critical misalignment angle that separates two pathways for bonding; below this critical angle gold nanocrystals can realign for defect-free coherent bonding and above which the defect is formed at the interface that mediates the bonding. Surprisingly, the distribution of the attachment events across different angles is not uniform and indicates that gold nanoparticles prealign prior to contact¹¹ (Supporting Information Figure S4 and Video S4). This prealignment (Figure 4B) suggests that solution-mediated entropic forces play a key role during the approach of nanocrystals prior to their bonding.^{36–38} Such investigations are underway.

Using *in situ* TEM and MD simulations, we have validated that bonding of gold nanocrystals is driven by surface energy

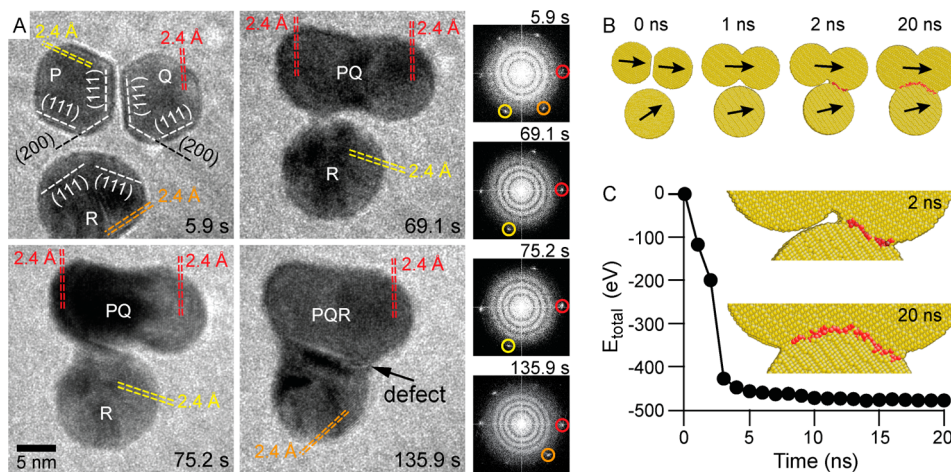


Figure 3. A mixed case: coherent and defect-mediated bonding between three gold nanocrystals. (A) Nanocrystals, *P* and *Q*, bond through a common (111) lattice plane forming a new defect-free nanocrystal, *PQ*. Next, crystal-*R* approaches (*t* = 69.1 s) and bonds (*t* = 75.2 s) with crystal-*PQ* through uncommon lattice planes ((200) and (111)). As a result final crystal *PQR* has a visible defect at the bonding interface between *R* and *PQ* (black arrow, *t* = 135.9 s). Observed lattice fringes in the images (dashed lines) and corresponding Fourier reflections (circled) of (111) planes are the same color. (Supporting Information Video S3). (B) MD simulations of bonding between three 10 nm gold nanocrystals show a coherent bonding between the two top oriented nanocrystals followed by defect-mediated bonding between bottom and newly formed top nanocrystals (arrows indicate the orientation of close-packed (111) planes). Defects in the crystal are indicated by red atoms. (C) Change in total energy during bonding between three nanocrystals. Inset is a zoomed in view of bonding interface between top and bottom nanocrystals shown in (B).

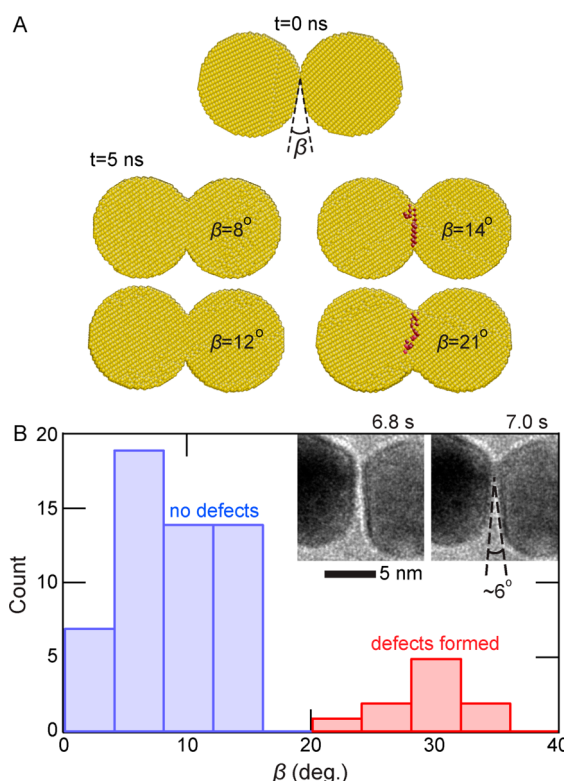


Figure 4. Nanocrystal bonding at different initial contact angles. (A) MD simulations for different angles at contact indicate that there is a critical misalignment angle between 12°–14° for the bonding of two gold nanocrystals. No defects are formed at the bonding interface for $\beta \leq 12^\circ$. (B) Histogram of experimental nanocrystal bonding events at different orientation angles (β) measured between the common (111) lattice planes at contact as shown in the inset. At $\beta \leq 15^\circ$, the bonding between two gold nanocrystals results in defect-free single nanocrystals, whereas, for angles between 20° and 35° clear persistent defects at the merging interface are observed.

that is always greater than the energy cost due to defect formation. Our direct observation of nanocrystal bonding in solution shows that there exists a critical attachment angle that separates defect-free coherent bonding from defect-mediated bonding. Ability to control the angle between two bonding nanocrystals may lead to effective rules for creating hierarchical nanocrystal-based structures.

■ ASSOCIATED CONTENT

Supporting Information

Supporting text, figures, and videos. This material is available free of charge via the Internet at <http://pubs.acs.org>.

■ AUTHOR INFORMATION

Corresponding Authors

*E-mail: (U.M.) phyumm@nus.edu.sg.
*E-mail: (H.S.) hbsu@ntu.edu.sg.

Author Contributions

Z.A., J.L., and X.Z. are equal contributors.

Notes

The authors declare no competing financial interest.

■ ACKNOWLEDGMENTS

This work was supported by the Singapore National Research Foundation's Competitive research program funding (NRF-CRP9-2011-04). The authors acknowledge the support of the Electron Microscopy Facility at Center for Bioimaging Science, National University of Singapore. N.D.L. thanks the support of the Lee Kuan Yew endowment fund.

■ REFERENCES

- Lim, B.; Jiang, M.; Camargo, P. H. C.; Cho, E. C.; Tao, J.; Lu, X.; Zhu, Y.; Xia, Y. *Science* **2009**, 324, 1302–1305.
- Banfield, J. F.; Welch, S. A.; Zhang, H.; Ebert, T. T.; Penn, R. L. *Science* **2000**, 289, 751–754.
- Cho, K. S.; Talapin, D. V.; Gaschler, W.; Murray, C. B. *J. Am. Chem. Soc.* **2005**, 127, 7140–7147.

- (4) Xue, X.; Penn, R. L.; Leite, E. R.; Huang, F.; Lin, Z. *CrystEngComm* **2014**, *16*, 1419–1429.
- (5) Tang, Z.; Kotov, N. A.; Giersig, M. *Science* **2002**, *297*, 237–240.
- (6) Zheng, H.; Smith, R. K.; Jun, Y.; Kisielowski, C.; Dahmen, U.; Alivisatos, A. P. *Science* **2009**, *324*, 1309–1312.
- (7) Zitoun, D.; Pinna, N.; Frolet, N.; Belin, C. *J. Am. Chem. Soc.* **2005**, *127*, 15034–15035.
- (8) Liao, H.-G.; Zherebetsky, D.; Xin, H.; Czarnik, C.; Ercius, P.; Elmlund, H.; Pan, M.; Wang, L.-W.; Zheng, H. *Science* **2014**, *345*, 916–919.
- (9) Murray, C. B.; Norris, D. J.; Bawendi, M. G. *J. Am. Chem. Soc.* **1993**, *115*, 8706–8715.
- (10) Yuk, J. M.; Park, J.; Ercius, P.; Kim, K.; Hellebusch, D. J.; Crommie, M. F.; Lee, J. Y.; Zettl, A.; Alivisatos, A. P. *Science* **2012**, *336*, 61–64.
- (11) Li, D.; Nielsen, M. H.; Lee, J. R. I.; Frandsen, C.; Banfield, J. F.; Yoreo, J. D. *Science* **2012**, *336*, 1014–1018.
- (12) Liao, H.-G.; Cui, L.; Whitelam, S.; Zheng, H. *Science* **2012**, *336*, 1011–1014.
- (13) Lu, Y.; Huang, J. Y.; Wang, C.; Sun, S.; Lou, J. *Nat. Nanotechnol.* **2010**, *5*, 218–224.
- (14) Grouchko, M.; Roitman, P.; Zhu, X.; Popov, I.; Kamyshny, A.; Su, H.; Magdassi, S. *Nat. Commun.* **2014**, *5*, 2994–2998.
- (15) Wang, Y.; Liang, W.; Geng, C. *Nanoscale Res. Lett.* **2009**, *4*, 684–688.
- (16) Penn, R. L.; Banfield, J. F. *Science* **1998**, *281*, 969–971.
- (17) Nielsen, M. H.; Li, D.; Zhang, H.; Aloni, S.; Han, T. Y.-J.; Frandsen, C.; Seto, J.; Banfield, J. F.; Cölfen, H.; De Yoreo, J. J. *Microsc. Microanal.* **2014**, *20*, 425–436.
- (18) Burton, W. K.; Cabrera, N.; Frank, F. C. *Nature* **1949**, *163*, 398–399.
- (19) Venables, J. A.; Giordano, L.; Harding, J. H. *J. Phys.: Condens. Matter* **2006**, *18*, S411–S427.
- (20) Kuhlmann-Wilsdorf, D. *Philos. Mag. A* **1999**, *79*, 955–1008.
- (21) White, W. M. *Geochemistry*; John Wiley & Sons: New York, 2013.
- (22) de Jonge, N.; Peckys, D. B.; Kremers, G. J.; Piston, D. W. *Proc. Natl. Acad. Sci. U.S.A.* **2009**, *106*, 2159–2164.
- (23) Grogan, J. M.; Schneider, N. M.; Ross, F. M.; Bau, H. H. *Nano Lett.* **2014**, *14*, 359–364.
- (24) Woehl, T. J.; Evans, J. E.; Arslan, I.; Ristenpart, W. D.; Browning, N. D. *ACS Nano* **2012**, *6*, 8599–8610.
- (25) White, E. R.; Mecklenburg, M.; Singer, S. B.; Aloni, S.; Regan, B. C. *Appl. Phys. Express* **2011**, *4*, 055201.
- (26) Mirsaidov, U. M.; Zheng, H.; Bhattacharya, D.; Casana, Y.; Matsudaira, P. *Proc. Natl. Acad. Sci. U.S.A.* **2012**, *109*, 7187–7190.
- (27) Liu, Y.; Lin, X.-M.; Sun, Y.; Rajh, T. *J. Am. Chem. Soc.* **2013**, *135*, 3764–3767.
- (28) White, E. R.; Mecklenburg, M.; Shevitski, B.; Singer, S. B.; Regan, B. C. *Langmuir* **2012**, *28*, 3695–3698.
- (29) Zheng, H.; Claridge, S. A.; Minor, A. M.; Alivisatos, A. P.; Dahmen, U. *Nano Lett.* **2009**, *9*, 2460–2465.
- (30) Lu, J.; Aabdin, Z.; Loh, N. D.; Bhattacharya, D.; Mirsaidov, U. *Nano Lett.* **2014**, *14*, 2111–2115.
- (31) Schneider, N. M.; Norton, M. M.; Mendel, B. J.; Grogan, J. M.; Ross, F. M.; Bau, H. H. *J. Phys. Chem. C* **2014**, *118*, 22373–22382.
- (32) Israelachvili, J. N. *Intermolecular and Surface Forces*, 3rd ed.; Academic Press: San Diego, 2011.
- (33) Ikeda, H.; Qi, Y.; Cagin, T.; Samwer, K.; Johnson, W. L.; Goddard, W. A. *Phys. Rev. Lett.* **1999**, *82*, 2900–2903.
- (34) Landman, U. *Proc. Natl. Acad. Sci. U.S.A.* **2005**, *102* (19), 6671–6678.
- (35) Kelchner, C. L.; Plimpton, S. J.; Hamilton, J. C. *Phys. Rev. B* **1998**, *58*, 11085–11088.
- (36) Roth, R.; van Roij, R.; Andrienko, D.; Mecke, K.; Dietrich, S. *Phys. Rev. Lett.* **2002**, *89*, 088301.
- (37) Park, K.; Koerner, H.; Vaia, R. A. *Nano Lett.* **2010**, *10*, 1433–1439.
- (38) Henzie, J.; Grünwald, M.; Widmer-Cooper, A.; Geissler, P. L.; Yang, P. *Nat. Mater.* **2012**, *11*, 131–137.